Journal of Nuclear Materials 510 (2018) 596–602

Contents lists available at ScienceDirect

Journal of Nuclear Materials

journal homepage: www.elsevier.com/locate/jnucmat

Ab initio study of the stability of intrinsic and extrinsic Ag point defects in 3C–SiC

Nanjun Chen [a], Qing Peng [a, *], Zhijie Jiao [a], Isabella van Rooyen [b], William F. Skerjanc [c], Fei Gao [a, *]

[a] Nuclear Engineering and Radiological Sciences, University of Michigan, Ann Arbor, MI, 48109, USA
[b] Fuel Design and Development Department, Idaho National Laboratory, Idaho Falls, ID, 83415-6188, USA
[c] Reactor Physics Design and Analysis Department, Idaho National Laboratory, Idaho Falls, ID, 83415-6188, USA

ARTICLE INFO

Article history:
Received 4 June 2018
Received in revised form
22 August 2018
Accepted 28 August 2018
Available online 29 August 2018

Keywords:
Fission product
Silicon carbide
Point defects
Density functional theory

ABSTRACT

We have systematically investigated the energetics and stability of Ag atom in 3C–SiC with various charge states using first-principles calculations within large supercells. Up to 18 Ag-defect configurations have been examined, including substitutionals, interstitials, and vacancy-based complexes. A general trend is that the formation energy of Ag-defect complexes is generally lower than interstitial typed defects. With the lowest formation energy, the configuration with Ag_T_{Si}-V_C^{3+} turns out to be the most stable one. It has also been found a neutral Ag is more likely to substitute a silicon lattice site with a nearest carbon vacancy, thus forming an Ag_{Si}-V_C pair. All these data are important inputs in the next coarser-level modeling to understand the Ag migration in and release from 3C–SiC under both thermal and radiation conditions.

1. Introduction

As a promising advanced next generation fission nuclear reactor, High Temperature Gas Reactor (HTGR) stands out over conventional nuclear reactors due to its high thermal efficiency and better ability in handling safety issues. The fuel applied in this reactor is in the form of coated spherical particles, which are known as Tri-structural isotropic (TRISO) particles [1]. This type of fuel has been studied extensively in recent years as it can effectively retain and contain fission products (FPs) to reduce the risk of leakage and coolant contamination [2]. An individual TRISO fuel particle is comprised of a UO_2/UC kernel, surrounded by a carbonaceous buffer layer and subsequent isotropic layers of pyrolytic carbon, silicon carbide (SiC), and outer pyrolytic carbon. One of the main functions of these coating layers is to act as diffusion barriers for radioactive fission products (FPs), thereby keeping these FPs within the fuel particles, even under accident conditions. However, among the four layers, silicon carbide is the most important one which has advantages that provide both structural support and dimensional stability and thus act as the primary diffusion barrier to prevent FPs release [3]. Among over 200 polytypes, cubic SiC (3C–SiC, zinc-blende structure) is the most stable type below 2373 K [4] which has been widely explored in structural applications of nuclear reactors [5].

While TRISO fuel has demonstrated excellent retention of fission products and radioisotopes, release of some fission products from intact fuel can still be observed from experiments under conditions similar to accident scenarios [6,7]. It has been shown in the past few decades that ^{110m}Ag can be released in higher concentrations than other fission products [8–10] and is able to diffuse through SiC [11–13]. Multiple experiments [14–16] have also been conducted to determine the existence and formation of Ag in SiC. The first direct evidence of Ag in a neutron irradiated SiC layer was reported by Van Rooyen et al. [14] utilizing several characterization techniques, i.e. scanning transmission electron microscopy (STEM). Significant concentrations of silver were identified in both grain boundaries and triple junctions in SiC layer near the edge of IPyC. Moreover, when 6H–SiC is implanted with 360 keV Ag^+ ions to a fluence of 2×10^{16} Ag^+ cm^{-2}, voids were obtained [16] to be filled with implanted Ag following thermal annealing in the range 1250 °C -1500 °C. Similar feature to the observation in 6H–SiC is also visible in β–SiC, where Ag particles are surrounded by voids with 400 keV Ag ion implantation at room temperature to a fluence of 2×10^{16}

* Corresponding authors.
E-mail addresses: qpeng@umich.edu (Q. Peng), gaofeium@umich.edu (F. Gao).

https://doi.org/10.1016/j.jnucmat.2018.08.053
0022-3115/

Ag^{+} cm^{-2} followed by annealing up to 1600 °C for 60 h [17]. However, faceted voids were not observed in as-implanted samples [17]. As suggested by the Rutherford Backscattering Spectroscopy channeling experiments [18], Xiao et al. reported that all the implanted Ag resided interstitially after implantation with 2.0 and 4.0 MeV Ag^{+} ions to an average flux of 1.7×10^{12} cm^{-2} s^{-1} at 375 °C, no substitution Ag was detected even for low-fluence samples.

Despite numerous experimental investigations on Ag formation in SiC, the basic knowledge of properties of defect associated with Ag at the atomic level is sparsely understood. Only a recent study by Shrader et al. [19] has revealed Ag defects formation in bulk SiC through first-principle calculations. They have concluded Ag_{Si}-V_C to be the most stable defect at Si-rich limit under n-type condition. But, their result still has its limitation in accuracy, as they have used a relatively small simulation block containing 64 atoms for an undefected SiC. Therefore, in present study, we decided to provide a more comprehensive and thorough insight into the stability of defects in SiC involved with Ag impurities, together with clustering and interactions with native defects, particularly in connection with diffusion in SiC. This could have great significance to serve as both the most accurate input and primary contribution to the exploration of general behavior of Ag in SiC. While density functional theory (DFT) [20] has emerged as the most powerful approach in so many areas of solid-state physics to identify and characterize impurities and defects in a number of materials, we thus apply *ab initio* calculations to a larger model of pristine SiC containing 216 atoms. Since defects can facilitate charge transfer to their surrounding atoms, such charge transfer to and from neighboring atoms will alter potential barriers and diffusion dynamics in the formation of stable defects [21]. Thus, charge states are also included in this investigation.

2. Method

2.1. Computational approach

Calculations in this work were all performed using the density function theory (DFT) as implemented in the Vienna Ab Initio Simulation Package (VASP) [22]. Accurate projected augmented wave (PAW) potentials [23] were applied with valence electrons explicitly including $4d^{10}5s^{1}$ for Ag, $3s^{2}3p^{2}$ for Si, and $2s^{2}2p^{2}$for C, respectively. The generalized gradient approximation (GGA) as parameterized by Perdew-Burke-Ernzerhof (PBE) was used for exchange-correlation [24]. The model of the pristine SiC introduced was a 3C—SiC supercell with a lattice constant of 4.36 Å, which was composed of $3 \times 3 \times 3$ unit cells with 216 atoms. For all the models considered, convergence tests guided a plane wave expansion cutoff energy of 500 eV. To sample the irreducible Brillouin Zone in the structure to preserve the symmetry, a $4 \times 4 \times 4$ Monkhorst-Pack k-points mesh was carefully chosen for convergence and accuracy. Conjugated-gradient was used to fully relax all atomic positions, cell shapes, and cell volume to achieve the minimum total energy of the systems. The total energy was required to reach the convergence to a small change within 1.0×10^{-5} eV/atom between two relaxation runs, while the Hellmann-Feynman forces were minimized until the maximum force on the ion was smaller than 0.01 eV/Å. The van der Waals interactions are described by the DFT-D3 [25] throughout this study. However, despite a good structural description including atom positions and cell parameters, the usual errors intrinsic to the DFT-GGA exist. The calculated band gap for SiC was strongly underestimated amounting up to 40% of the experimental value (1.43 vs. 2.2—2.4 eV [26,27]), which is a typical issue of the DFT "band-gap problem" [28,29]. Even though there are a variety of approaches to achieve the band-gap correction, the hybrid functional has shown a great promise to alleviate the underestimation due to the moderate computational cost and robust reliability method [28,30]. Here, the correction of the band gap has been performed by Heyd-Scuseria-Ernzerhof (HSE) hybrid functional [31,32], and the band gap has now been corrected to 2.295 eV, with this functional, which fits well with the experimental data.

2.2. Calculation of formation energy

In order to evaluate the energetic stability of these defects, we define the formation energy of the Ag-related defects in a charge state q as follow [33]:

$$E_f^q = E_{defect} - E_{perfect} - \mu_{Ag} + \sum_{X=1}^{2} n_X \mu_X + q\left(E_{VBM} + \left(E_1^{core} - E_0^{core}\right) + \mu_F\right) + E_{MP}, \quad (1)$$

$n_X = 1$, one X atom is removed;
$n_X = 0$, no change in the number of X atom;
$n_X = -1$, one X atom is added;

where E_{defect} is the total energy of a supercell containing a defect in charge state, q and $E_{perfect}$ is the total energy of a perfect 3C—SiC supercell, respectively. The integer n_X indicates the number of atoms of type X added to ($n_X < 0$) or removed from ($n_X > 0$) the supercell to form the defects. The μ_X (X = Si or C) is the corresponding atomic chemical potential describing exchange of particles with respective reservoir. The chemical potential of silver (μ_{Ag}) was calculated from a bulk crystal of silver. Electrons added or removed from the supercell are exchanged with the Fermi level, μ_F of the semiconductor host which is referenced to the valence-band maximum, E_{VBM}. The term (E_1^{core}-E_0^{core}) is electronic potential shift. The E_{MP} is a charge correction term in periodic boundary conditions due to the finite size of the supercell which is handled by Makov and Payne [34].

2.3. Charge-state transition levels

Most point defects are electrically active defects, which can exist in several different charge states, depending on the position of the Fermi level. As the Fermi level is raised, defect-induced states within the band gap become filled with electrons. A certain charge state is now realized if its formation energy $E_f^q(\mu_F)$ for a given Fermi level μ_F is lower than that of all other charge states. The commonly considered defect level corresponds to the Fermi-level positions where a transition from one charge state to another one occurs. Technically, these levels are defined as "thermodynamic transition levels," and they correspond to the Fermi-level positions where the formation energies of two charge states of a defect are equal [35]. Then, the value of the Fermi energy μ_F where the dominating charge state changes from q to q' is described as

$$\varepsilon(q/q') = \frac{E_f^{q'} - E_f^q}{q - q'} \quad (2)$$

where $E_f^{q'}$ and E_f^q are the formation energies of a defect in charge state q′ and q, respectively, when Fermi level is at valence band maximum (VBM). Here, we neglect the pressure- and temperature-dependent terms in the formation enthalpy of the defects. Accurate

calculation of these levels is essential for defect identification and characterization.

3. Results and discussion

3.1. Chemical potential

Chemical potentials represent the energy of the reservoirs with which atoms are being exchanged. More generally, the defect formation energy is dependent on the chemical potential of an atomic constituent as well as electron chemical potential. Therefore, the formation energy of a defect can depend on the chemical potential of Si, C, and electrons. In current work, the chemical potential of silver was calculated from its stable crystal structure (face-centered structure) at room temperature, while C and Si were calculated from a zinc-blende structure. For the chemical potentials of Si and C in bulk SiC, they were derived under equilibrium constraints and with a wide range of values for a species X (Si or C) of, $E_f < \mu_X < E_X$ (where $E_f = E_{SiC} - E_{Si} - E_C$, is the *ab initio* formation energy of SiC). E_X is defined as *ab initio* energy of bulk phase of species X, while E_{SiC} is *ab initio* energy of bulk SiC, where $E_{SiC} = \mu_{Si} + \mu_C$. In Si rich limit, the chemical potential of Si is calculated in its bulk phase (cubic Si), and $E_{SiC} - \mu_{Si}(\text{bulk}) = \mu_C$. In C rich limit, the chemical potential of C is calculated in its bulk phase (graphite), and $E_{SiC} - \mu_C(\text{bulk}) = \mu_{Si}$. The Si and C rich cases can provide bounds on the formation energy with respect to Si and C reservoir chemical potential ranges. For consistency (possible comparison) with the majority of the reference literature [33,37], all defect energies reported in the current work are for Si-rich condition in p-type reference state, in which Fermi energy is assumed to be at the valance-band edge ($\mu_F = E_{VBM}$). The calculated chemical potential of impurity atoms and 3C–SiC are given in Table 1.

3.2. Energetics of intrinsic point defects in 3C–SiC

To study the stability of silver in 3C–SiC, we started to investigate the native point defect properties in SiC. Even though there are plenty of comprehensive works, which have dealt with defect study in SiC [37–40], the similar simulation carried out here is aiming for comparison and model validation purposes. As SiC is a compound semiconductor, there should be two different tetrahedral interstitial sites. One is tetrahedrally coordinated with four surrounding silicon atoms and another is associated with four carbon neighbors. They are denoted as T_{Si} and T_C, respectively. Followed by the similar rule, possible defects such as antisites, interstitials and defect complexes can be constructed by any combination of Si and C on the its relative sub-lattices. Particularly, the formation energies of fifteen defects in several charge states were considered in the current work, which are listed in Table 2. Here, we refer to formation energies in silicon-rich conditions, unless stated otherwise. The notation of the defects is also defined for simplicity, where <100>, <110>, <111> denote the split interstitials along <100>, <110>, and <111> directions, respectively. Comparing the results from our work and other calculations from literature [19,37–39], the energetics, as well as the stability order, agree with each other excellently. For example, the general order of the interstitial stability as compared with Ode et al. [36] is similar. Starting from the most stable to the least stable, the order can be listed as C–C<100>, C–C<110>, C_T_{Si}, and C_T_C for carbon interstitials in both neutral and 2 + charge state; Si_T_C, Si<100>, Si_T_{Si}, and Si–Si<100> for silicon interstitials in 2 + charge state. However, the energy order of Si_T_C and Si–Si<110> in the neutral state is controversial due to the limitations of k-point sampling and/or a supercell size [41]. Overall, the model we used is fairly supported by the calculated results.

Table 1
Chemical potentials for the considered impurities, Si and C in 3C–SiC (unit = eV).

μ	DFT (Present)	[36]	[33]
Ag	−3.2972	−2.95	
C	−9.0930		−9.20
Si	−5.4203		−5.44
SiC	−15.0612		−15.08
Si (Si_rich)	−5.7372		−5.44
C (Si_rich)	−9.9244		−9.65
Si (C_rich)	−6.2956		−5.89
C (C-rich)	−9.3660		−9.20

3.3. Stability of silver in 3C–SiC

One of the crucial quantities relevant to the evaluation of the thermodynamic and kinetic behaviors of impurity in solid solution is the formation energy of impurity-related defects. When an isolated silver impurity is inserted in the bulk SiC, various defects could be formed associated with a silver atom. Some of them can be distinguished by a carbon-like or silicon-like defects. Here, we have investigated up to eighteen important configurations that are likely to form in the bulk SiC. They can be classified into three categories, including an impurity substitution, an impurity as an interstitial, and a defect complex with a nearby vacancy. For example, in interstitial type, Ag can be located at a tetrahedral site surrounded by either four silicon or carbon neighbors (denoted as Ag_T_{Si} or Ag_T_C). Split interstitials also exist when a silver atom shares a lattice site with a host atom. These split interstitials can be either dumbbell or crowdion oriented in <100>, <110>, and <111>. For defect complexes, tetrahedral-vacancy configurations and substitution-vacancy configurations are considered. In a tetrahedral-vacancy complex, Ag is tetrahedrally coordinated within the cage of four carbon (silicon) atoms with a vacant site being either the nearest neighbor or the next nearest neighbor to the same sub-lattice. However, in a substitution-vacancy complex, one lattice site is occupied by a Ag atom with one of the nearest or the second nearest neighbor being vacant. Since the defect configurations associated with Si are similar to C, only defect configurations with respect to silicon sub-lattice are illustrated in Fig. 1(a)–(g).

To obtain a comprehensive study of the stability of silver in 3C–SiC, we calculated formation energy for multiple defects in seven charged states (3-, 2-, 1-, 0, 1+, 2+, 3+). For a given defect configuration, the stable structure was taken after fully relaxation of cell parameters, ion positions, and electronic structure. Hence, the formation energy and transition level of defects in 3C–SiC that are resulted from different defects are both included in this section. The defect formation energies are summarized in Table 3, where the results from Shrader's 64-atom supercell case [19] are included for comparison. Fig. 2(a)–(c) demonstrate the formation energies for Ag related defects in SiC as a function of Fermi-level position within the band gap. Note that the formation energies of charged defects depend on the position of VBM which has been evidenced in Eq. (1). The kinks in the curve for a given defect indicate transitions between different charge states.

3.3.1. Substitutions

Occupation of carbon or silicon site by a silver atom leads to the substitution type of defect. In neutral state, the energetic order of a Ag substituting Si and C indicates that Ag would be more likely to occupy a Si site. The charge states of these substitution defects in different ranges from Fermi level are indicated under Si-rich condition in Fig. 2(a). Both defects exhibit six charge-state transition levels. When the Fermi level lies closer to VBM, the formation of

Table 2
Intrinsic defect formation energy (eV) in 3C–SiC.

Defect	−3	−2		−1		0		1		2		3	
	Current	Current	Other cal.	Current	Other cal.	Current	Other cal.	Current	Other cal.	Current	Other cal.	Current	Other cal.
V_C	9.61	7.78	8.1[b]	5.98	5.6[b]	4.23	4.19[a],4.1[b]	2.54	2.74[a],2.8[b]	1.02	1.73[a],2.1[b]	1.08	
V_{Si}	11.57	10.06	9.75[a],10.6[b]	9.10	8.15[a],9.0[b]	8.40	7.63[a],8.5[b]	6.74	7.58[a],8.5[b]	7.69	9.4[b]	7.84	
Si_C	8.68	6.76	8.1[b]	4.94	5.3[b]	3.37	3.56[a],3.5[b]	−1.75	3.45[a],3.5[b]	11.29	4.2[b]	2.85	
C_{Si}	9.28	7.43	8.9[b]	5.66	6.1[b]	4.16	4.03[a],4.4[b]	3.14	4.9[b]	12.37	6.2[b]	20.54	
C_T_C	16.50	10.36		9.05		11.16		9.93		7.88		6.86	
C_T_{Si}	15.29	13.55		11.89		10.32		9.38		7.53		7.51	
Si_T_C	14.19	11.66		10.12		8.21		13.04		4.58		2.89	
Si_T_{Si}	16.09	14.00		11.98		10.04		6.35		6.55		5.32	
C–C<100>	12.75	10.88	11.8[b]	9.05	9.2[b]	7.33	6.95[a],7.5[b]	5.79	5.81[a],6.3[b]	4.46	5.17[a],5.6[b]	4.44	
C–C<110>	12.35	10.59		8.97		7.51		6.27		5.11		5.08	
C–C<111>	27.01	25.08		23.20		21.38		19.64		18.12		17.11	
Si–Si<100>	14.72	12.94		11.26		9.67		8.18		6.91		2.89	
Si–Si<110>	14.18	12.11	14.0[b]	10.12	10.9[b]	8.35	8.75[a],8.6[b]	7.28	7.81[a],7.5[b]	6.32	7.32[a],7.5[b]	5.48	
Si–Si<111>	22.73	20.85		19.02		17.31		15.99		14.35		12.94	
C_{Si}-V_C	13.39	11.62		10.03		8.39	7.24[c]	7.94		5.25		5.34	

[a] Reference [19].
[b] Reference [37].
[c] Reference [38].

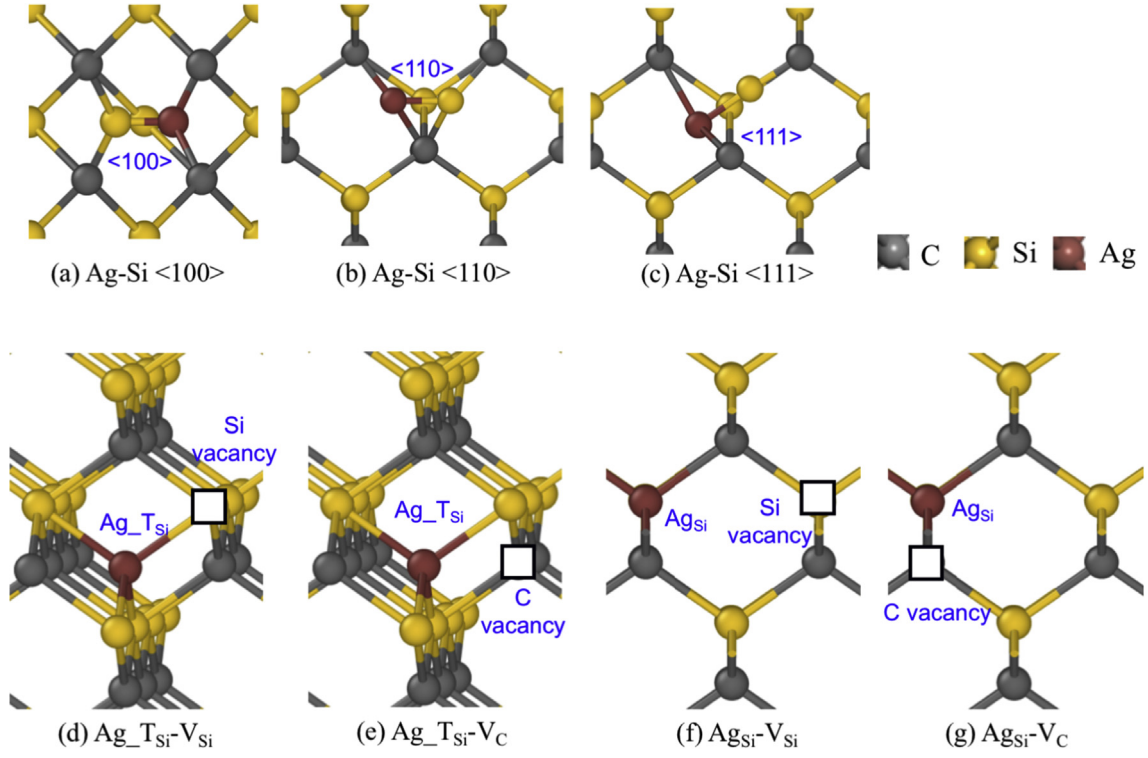

Fig. 1. Geometry of the Ag-related defect in SiC. The gray sphere denotes carbon atom, yellow stands for Si, and the red one indicates Ag. (a). Configuration of a Ag–Si <100> interstitial; (b). Configuration of a Ag–Si <110> interstitial; (c). Configuration of a Ag–Si <111> interstitial; (d) Ag at the tetrahedral position surrounding by four Si atoms and a Si vacancy (Ag_T_{Si}-V_{Si}); (e). Ag at the tetrahedral position surrounding by four Si atoms with a nearby C vacancy (Ag_T_{Si}-V_C); (f) A silicon substitution by Ag atom with a second nearest neighbor Si vacancy (Ag_{Si}–V_{Si}); (g). A silicon substitution by a Ag atom with a first nearest neighbor C vacancy (Ag_{Si}-V_C). (For interpretation of the references to colour in this figure legend, the reader is referred to the Web version of this article.)

silver substituting a carbon site is energetically favorable relative to the formation of substituting a silicon site. The figure indicates that Ag_C is the most stable in charge state 3 + ranging from VBM to 1.56 eV above VBM. The transition between 3 + and 2 + states locates at 1.56 eV. As silver atom is over twice larger than carbon atom and 0.5 Å larger than Si in size [42], Ag prefers carbon site at positive charge which presents a smaller size by removing electron from Ag. The transition between 3 + and 2 + states locates at 1.56 eV, which is slightly over mid-gap. Therefore, the addition of electron to V_C^{3+} causes partial occupation of the conduction band. In Si-rich limit, the formation energy of Ag_{Si} is much lower, in which μ_F is close to conduction band maximum (CBM), indicating that the Si site is likely to be occupied by Ag. A transition between 2- and 3- of this defect occurs at 1.045 eV below CBM. Different from the characteristics of Ag_C, Ag_{Si} stably exists at Fermi-level positions near CBM with a negative charge of 3-. Opposite explanation to aforementioned Ag_C is applicable for the existence of Ag_{Si} in which larger Ag prefers Si site with negative charge. When Fermi level

Table 3
Formation energy (eV) of Ag-related defects in SiC at Si-rich limit under p-type doping condition in seven charge states.

Defect	−3		−2		−1		0		1		2		3	
	Current	[19]	Current	[19]	Current	[19]	Current	[19]	Current	[19]	Current	[19]	Current	[19]
Ag_C	12.98		11.01		9.07		7.23	7.39	5.51	5.71	3.87	4.62	2.33	4.01
Ag_{Si}	10.04	10.87	8.82	8.9	7.81	7.89	7.03	6.60	6.48	6.31	6.15		5.98	
Ag_T_C	15.89		13.82		11.81		9.89	10.49	8.22	8.78	8.09		8.04	
Ag_T_{Si}	16.77		14.75		12.79		10.92	11.38	9.31	9.81	9.02		8.95	
Ag−C<100>	16.77		14.75		12.79		10.92		9.31		9.02		8.85	
Ag−C<110>	15.26		13.32		11.60		9.89		8.26		7.88		7.67	
Ag−C<111>	21.69		19.75		17.86		16.05		14.44		13.60		12.93	
Ag−Si<100>	15.89		13.82		11.81		9.89		8.22		8.09		8.04	
Ag−Si<110>	15.57		13.63		11.90		10.51	10.91	9.18	9.79	8.70	9.68	8.40	
Ag−Si<111>	15.72		13.77		12.04		9.88		9.53		7.89		8.71	
Ag_{Si}-V_C	9.33		7.52		5.97	5.85	5.55	5.32	5.28	5.3	5.14		5.11	
Ag_{Si}−V_{Si}	12.87	17.16	11.17	15.36	9.66	14.19	8.97	13.53	8.50		8.25		8.16	
Ag_C-V_C	13.87		11.89		9.99		8.16		6.56	7.1	5.38	6.41	4.15	6.14
Ag_C−V_{Si}	9.33		7.52		5.97	5.85	5.55	5.32	5.28	5.3	5.14		5.11	
Ag_T_C-V_C	12.84		10.88		9.00		7.20		5.49		3.87		2.33	
Ag_T_C-V_{Si}	10.04		8.80		7.79		6.99		6.48		6.15		5.98	
Ag_T_{Si}-V_C	12.63		10.66		8.84		7.12		5.45		3.86		2.32	
Ag_T_{Si}-V_{Si}	20.23		18.87		17.66		16.68		15.90		15.30		14.89	

positioned above E_V+1.285 eV, Ag prefers to occupy the Si site rather than the C site. Beyond this range, Ag is favorable on the C site.

3.3.2. Interstitials

The Ag interstitials in 3C−SiC have been thoroughly investigated as well. Technically, there are eight configurations investigated in this work as aforementioned, but only six out of eight are mechanically stable after fully relaxation, including Ag_T_C, Ag_T_{Si}, Ag−C<110>, Ag−C<100>, Ag−Si<110>, and Ag−Si<111>. Several structures have also observed an undistinguishable characteristic for a certain Fermi-level range as illustrated in Fig. 2(b). In general, the formation energy decreases with increasing the positive charge states because energy is gained by promoting electrons from the defect to the Fermi level if the defect is below the Fermi level. Likewise, if Fermi level lies higher, the formation energy also decreases with decreasing the negatively charged states, as the energy is gained by the promoting electrons from the Fermi level to the defect. The neutral state of all the defects shows the highest formation energy as compared with other stable charge states in different Fermi level positions. For most interstitials, the defect in charge state 1 + holds the longest stability window of up to 1.5 eV. Ag_T_C is fairly low in formation energy which indicates the defect concentration of this type of interstitial in bulk is high when the system is neutral. At the valence band maximum, Ag and C are most likely to form a split interstitial oriented in the <110> direction in the 3 + charge state with the lowest formation energy among all the interstitials. This defect could exist from charge state 3 + to 3- in various Fermi level positions. Its (2-/3-) occupation level locates at E_V+1.94 eV, while (3+/2+) occupation level is almost degenerated with VB edge. In p-type condition, the Ag−Si<111> split interstitial is less stable than Ag−C<110>. Varying the electronic chemical potential, it exists only in the charge states 3-, 2-,1-, 0, and 2 + in 3C−SiC. The destabilization of charge state 1 + indicates an attractive effective electron-electron interaction and ionization level 1+/0 appears below 2+/1+, which is known as the negative-U effect [43,44]. This effect in the Ag−Si<111> mainly results from an enhanced electron-phonon coupling found for Ag−Si$<111>^{2+}$ and Ag−Si$<111>^{0}$. From 1+/0 and 2+/1 + transition levels, we find $U = \varepsilon(1+/0) - \varepsilon(2+/1+) = -1.29$ eV, which means the 1 + charge state is always higher in energy than the 2 + and neutral states. Therefore, the negative-U behavior amounts to 1.29 eV (Ag−Si$<111>^{1+}$).

3.3.3. Defect clusters

Since a single Ag atom could be an acceptor and a V_C is a donor in SiC, we would expect them to attract and form more complex configurations. We have also investigated the complexes of $Ag_{Si(C)}$ and Ag_T_{Si}(T_C) with a carbon or silicon vacancy. In all charge states, a combination of a Ag atom at a tetrahedral site which is surrounded by four Si atoms (T_{Si}) associated with a first nearest C vacancy (Ag_T_{Si}-V_C) in charge 3 + was observed to be the most stable with a formation energy of 2.32 eV. In the neutral state, it is noticeable that the lowest value of formation energy is of 5.55 eV for a defect configuration shown in Fig. 1(g), i.e., a Si atom substituted by an Ag coupled with a nearest neighbor C vacancy (Ag_{Si}-V_C). Another defect complex of a Ag in carbon sub-lattice with a nearby Si vacancy (denoted as Ag_C−V_{Si}) has shown an identical energetic level in all relevant charge states. Actually, the two complexes do not possess their initial configurations after fully relaxation. As a result, the Ag atom decays to the nearest neighbor vacancy. The final configurations for these two defects are eventually geometrically identical, thus resulting in the same formation energies in all charge states. Therefore, we take Ag_{Si}-V_C to be representative of the most stable defect complexes as the Ag is closer to a Si site. Comparing the formation energies of Ag_{Si} (7.03 eV), C vacancy (4.23 eV) and Ag_{Si}-V_C (5.55 eV), it can be concluded that there is a strong tendency for Ag_{Si} and C vacancy to form Ag_{Si}-V_C when both defects exist. Even after very high-temperature annealing, V_C can be trapped by Ag_{Si} as the energy barrier for an isolated carbon vacancy to diffuse is over 4 eV [45]. Coward et al. [17] has revealed the presence of voids around Ag particles in their annealed samples which could be associated with the low formation energy of the vacancy-substitution defect complex we explored here. Since void formation was not observed in the as-implanted samples in their experiments, a possibility of void mediated diffusion of the fission product transport mechanism was suggested. Thus, this strongly bounded complex could also be potentially important for the analysis of vacancy mediated diffusion. Moreover, among all the available configurations, a combination of a Ag_T_C associated with a first nearest Si vacancy (Ag_T_C-V_{Si}) turns out to be also a relatively low-energy defect structure with a formation energy of 6.99 eV in the neutral state (Si-rich condition). Compared to other defects, this defect complex is only less stable than Ag_{Si}-V_C, and may also play an important role in the diffusion landscape of silver in SiC.

Nevertheless, due to the wide band-gap of SiC, the formation

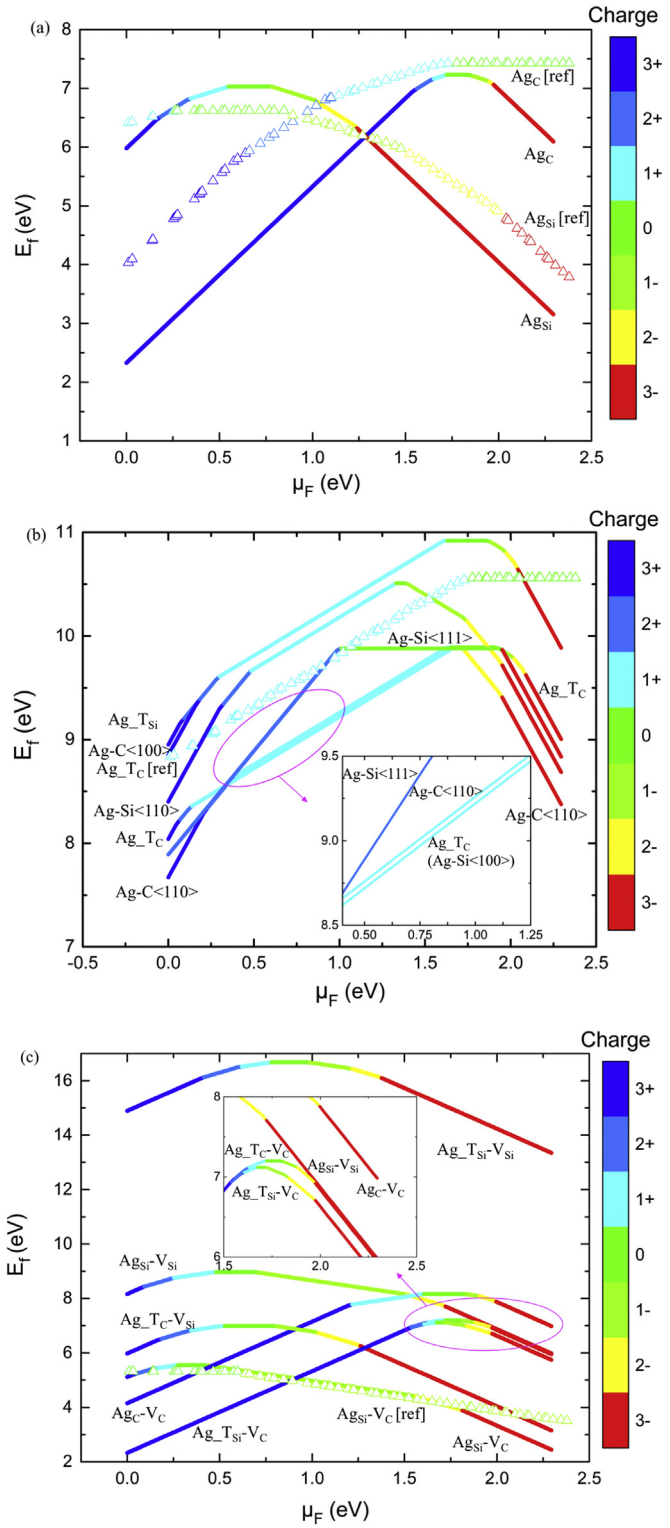

Fig. 2. Formation energies of Ag-related defects as a function of Fermi level position. (a) substitution-typed defect; (b) interstitial-typed defect; (c) defect complexes. Data cited (denoted with [ref]) was taken from Ref. [19].

energy of a charged complex can also vary strongly up to several eVs, depending on the position of the Fermi level as depicted in Fig. 2(c). According to our findings, Ag_T_{Si}-V_C is stable in all the charge states considered, while the Ag_T_{Si}-V_C^{3+} presents the lowest formation energy (2.32 eV) when the Fermi energy lies close to the VBM. This means that the defect complex can be stable as donor near VBM indicating that it can play an important role as compensating center in p-type SiC. However, in n-type SiC, in which μ_F is close to CBM, the formation of Ag_T_{Si}-V_C is electrically inactive. Even though Ag_T_C-V_C is almost identical to Ag_T_{Si}-V_C in positive charge states as illustrated in Fig. 2(c), it is still distinguishable at certain Fermi level between mid-gap and conduction band minimum. In neutral and negative charge states, Ag can then be stably located at T_C site which demonstrates a weaker binding with carbon vacancy as compared with Ag_T_{Si}-V_C with a higher energy level. Besides, at CBM, the defect complex Ag_{Si}-V_C is much more energetically favorable as compared with other clusters in n-type condition. In this complex, we also found a long stable window in a charge state 1- for the Ag_{Si}-V_C complex. Due to the ionicity of SiC [46], the substitutional defect when Ag is on Si site is more energetic favorable in negative charge states in which it compensates the missing electrons from surrounding carbon atoms as illustrated in Fig. 2(a), showing a longest window in 3- state. When a nearest carbon atom of this defect is removed from its lattice site, the supply to the missing electrons is mitigated, thus, shortening the existence of 3- state. The (1-/2-) transition level occurs at 1.56 eV above the VBM, and the 0/1- level is at 0.43 eV. In comparison with the result from Shrader's work, the calculated ionization level 0/1- agrees to within 0.2 eV. However, there are also some disagreements between our results and Shrader's calculations, especially for Ag_{Si}—V_{Si}. The formation energies of this defect complex from their calculations lie much higher in both neutral and negative charge states than the values we obtained in a 216-atom cell. Overall, the results confirm that the defect complexes associated with vacancies are much more stable than the interstitial-typed defects.

4. Conclusion

First-principles simulations were carried out to determine the formation energies of a number of intrinsic point defects and Ag-related defects at different charge states in 3C—SiC. We considered the chemical environments of Si-rich condition and charged or neutral states. We have found that Ag preferably substitutes a carbon lattice site in a charge state 3+, rather than a silicon site. The Ag impurity atom can also form thermally stable complexes with a carbon or a silicon vacancy. Among them, the Ag_T_{Si}-V_C^{3+} is the most stable one. The Ag_{Si}-V_C also turns out to be stable in its neutral state. However, the formation of Ag-related interstitial typed defects is less likely to be energetically stable as their formation energies are much higher than other defect types. Even though the interstitial typed defects are energetically unfavorable, they are also important, as abundant point defects including vacancies and interstitials, which are inevitably introduced by radiation. Consequently, the formation energies of various defects and their complexes from current DFT calculations could provide key parameters for understanding the behavior of Ag under both thermal and irradiation conditions in 3C—SiC crystal.

Acknowledgements

The authors would like to acknowledge the generous financial support from Nuclear Energy University Program program [grant numbers DE-NE0008519]. The authors would also like to acknowledge Dr. Gary Was for valuable discussions and critical comments.

Appendix A. Supplementary data

Supplementary data related to this article can be found at

https://doi.org/10.1016/j.jnucmat.2018.08.053.

References

[1] J.J. Powers, B.D. Wirth, A review of TRISO fuel performance models, J. Nucl. Mater. 405 (2010) 74–82.
[2] J.M. Beck, L.F. Pincock, High Temperature Gas-cooled Reactors Lessons Learned Applicable to the Next Generation Nuclear Plant, INL/EXT-10-19329, Idaho National Laboratory, Idaho Falls, Idaho, 2011.
[3] J.J. Van der Merwe, Evaluation of silver transport through SiC during the German HTR fuel program, J. Nucl. Mater. 395 (2009) 99–111.
[4] L.L. Snead, T. Nozawa, Y. Katoh, T.S. Byun, S. Kondo, D.A. Petti, Handbook of SiC properties for fuel performance modeling, J. Nucl. Mater. 371 (2007) 329–377.
[5] Y. Katoh, L.L. Snead, I. Szlufarska, W.J. Weber, Radiation effects in SiC for nuclear structural applications, Curr. Opin. Solid State Mater. Sci. 16 (2012) 143–152.
[6] R.N. Morris, D.A. Petti, D.A. Powers, B.E. Boyack, TRISO-Coated Particle Fuel Phenomenon Identification and Ranking Tables (PIRTs) for Fission Product Transport Due to Manufacturing, Operations, and Accidents: Main Report, 2004, p. 1. NUREG/CR-6844.
[7] P.A. Demkowicz, J.D. Hunn, S.A. Ploger, R.N. Morris, C.A. Baldwin, J.M. Harp, P.L. Winston, T.J. Gerczak, I.J. van Rooyen, F.C. Montgomery, C.M. Silva, Irradiation performance of AGR-1 high temperature reactor fuel, Nucl. Eng. Des. 306 (2016) 2–13.
[8] R.E. Bullock, Fission-product release during postirradiation annealing of several types of coated fuel particles, J. Nucl. Mater. 125 (1984) 304–319.
[9] P. Demkowicz, J.D. Hunn, R.N. Morris, J.M. Harp, P.L. Winston, C.A. Baldwin, F.C. Montgomery, S.A. Ploger, I.J. van Rooyen, Preliminary Results of post-irradiation Examination of the AGR-1 TRISO Fuel Compacts, No. INL/CON-12-24427, Idaho National Laboratory (INL), 2012.
[10] K. Minato, K. Sawa, T. Koya, T. Tomita, A. Iahikawa, C.A. Baldwin, W.A. Gabbard, C.M. Malone, Fission product release behavior of individual coated fuel particles for high-temperature gas-cooled reactors, Nucl. Technol. 131 (2000) 36–47.
[11] H. Nabielek, P.E. Brown, P. Offermann, Silver release from coated particle fuel, Nucl. Technol. 35 (1977) 483–493.
[12] E.L. Honorato, H. Zhang, P. Xiao, Investigation of Ag Diffusion in SiC, 2008.
[13] E.L. Honorato, H. Zhang, D. Yang, P. Xiao, Silver diffusion in silicon carbide coatings, J. Am. Ceram. Soc. 94 (2011) 3064–3071.
[14] I.J. van Rooyen, T.M. Lillo, Y.Q. Wu, Identification of silver and palladium in irradiated TRISO coated particles of the AGR-1 experiment, J. Nucl. Mater. 446 (2014) 178–186.
[15] T.M. Lillo, I.J. van Rooyen, J.A. Aguiar, Silicon carbide grain boundary distributions, irradiation conditions, and silver retention in irradiated AGR-1 TRISO fuel particles, Nucl. Eng. Des. 329 (2018) 46–52.
[16] J.B. Malherbe, Diffusion of fission products and radiation damage in SiC, J. Phys. D Appl. Phys. 46 (2013) 473001.
[17] R.A. Coward, C.R. Winkler, W.A. Hanson, M.L. Jablonski, M.L. Taheri, Transmission electron microscopy investigation of Ag diffusion mechanisms in β-SiC, J. Nucl. Mater. 457 (2015) 298–303.
[18] H.Y. Xiao, Y. Zhang, L.L. Snead, V. Shutthanandan, H.Z. Xue, W.J. Weber, Near-surface and bulk behavior of Ag in SiC, J. Nucl. Mater. 420 (2012) 123–130.
[19] D. Shrader, S.M. Khalil, T. Gerczak, T.R. Allen, A.J. Heim, I. Szlifarska, D. Morgan, Ag diffusion in cubic silicon carbide, J. Nucl. Mater. 408 (2011) 257–271.
[20] W. Kohn, L.J. Sham, Self-consistent equations including exchange and correlation effects, Phys. Rev. 140 (1965). A1133.
[21] F. Gao, H. Xiao, X. Zu, M. Posselt, W.J. Weber, Defect-enhanced charge transfer by ion-solid interactions in SiC using large-scale ab initio molecular dynamics simulations, Phys. Rev. Lett. 103 (2009), 027405.
[22] G. Kresse, J. Furthmüller, Efficiency of ab-initio total energy calculations for metals and semiconductors using a plane-wave basis set, Comput. Mater. Sci. 6 (1996) 15–50.
[23] P.E. Blöchl, Projector augmented-wave method, Phys. Rev. B 50 (1994) 17953.
[24] J.P. Perdew, K. Burke, M. Ernzerhof, Generalized gradient approximation made simple, Phys. Rev. Lett. 77 (1996) 3865–3868.
[25] S. Grimme, J. Antony, S. Ehrlich, H. Krieg, A consistent and accurate ab initio parametrization of density functional dispersion correction (DFT-D) for the 94 elements H-Pu, J. Chem. Phys. 132 (2010) 154104.
[26] R.G. Humphreys, D. Bimberg, W.J. Choyke, Wavelength modulated absorption in SiC, Solid State Commun. 39 (1981) 163–167.
[27] H. Morkoc, S. Strite, G.B. Gao, M.E. Lin, B. Sverdlov, M. Burns, Large-band-gap SiC, III-V nitride, and II-VI ZnSe-based semiconductor device technologies, J. Appl. Phys. 76 (1994) 1363–1398.
[28] W. Chen, A. Pasquarello, First-principles determination of defect energy levels through hybrid density functionals and GW, J. Phys.-Condens. Mat. 27 (2015) 133202.
[29] S. Lany, A. Zunger, Accurate prediction of defect properties in density functional supercell calculations, Model. Simul. Mater Sc. 17 (2009), 084002.
[30] B.J. Lynch, D.G. Truhlar, How well can hybrid density functional methods predict transition state geometries and barrier heights? J. Phys. Chem. A 105 (2001) 2936–2941.
[31] J. Heyd, G.E. Scuseria, M. Ernzerhof, Hybrid functionals based on a screened Coulomb potential, J. Chem. Phys. 118 (18) (2003) 8207–8215.
[32] J. Heyd, G.E. Scuseria, M. Ernzerhof, Erratum: hybrid functionals based on a screened Coulomb potential, J. Chem. Phys. 124 (2006) 219906.
[33] S. Hu, W. Setyawan, R.M. Van Ginhoven, W. Jiang, C.H. Henager Jr., R.J. Kurtz, Thermodynamic and kinetic properties of intrinsic defects and Mg transmutants in 3C-SiC determined by density functional theory, J. Nucl. Mater. 448 (2014) 121–128.
[34] G. Makov, M.C. Payne, Periodic boundary conditions in ab initio calculations, Phys. Rev. B 51 (1995) 4014.
[35] J.L. Lyons, C.G. Van de Walle, Computationally predicted energies and properties of defects in GaN, NPJ Comp. Mater. 3 (2017) 12.
[36] C. Kittel, P. McEuen, Introduction to Solid State Physics, seventh ed., Wiley, New York, 1996.
[37] P.C. Schuck, D. Shrader, R.E. Stoller, Ab initio study of palladium and silicon carbide, Philos. Mag. A 91 (2011) 458–467.
[38] F. Bernardini, A. Mattoni, L. Colombo, Energetics of native point defects in cubic silicon carbide, Eur. Phys. J. B 38 (2004) 437–444.
[39] T. Oda, Y. Zhang, W.J. Weber, Study of intrinsic defects in 3C-SiC using first-principles calculation with a hybrid functional, J. Chem. Phys. 139 (2013) 124707.
[40] F. Gao, E.J. Bylaska, W.J. Weber, L.R. Corrales, Ab initio and empirical-potential studies of defect properties in 3C–SiC, Phys. Rev. B 64 (2001) 245208.
[41] T. Liao, G. Roma, J. Wang, Neutral silicon interstitials in silicon carbide: a first principles study, Philos. Mag. A 89 (2009) 2271–2284.
[42] J.C. Slater, Atomic radii in crystals, J. Chem. Phys. 41 (1964) 3199–3204.
[43] G.D. Watkins, Negative-U properties for defects in solids, Adv. Solid State Phys. (1984) 163–189. Springer, Berlin, Heidelberg.
[44] P.W. Anderson, Model for the electronic structure of amorphous semiconductors, Phys. Rev. Lett. 34 (1975) 953–955.
[45] F. Gao, W.J. Weber, M. Posselt, V. Belko, Atomistic study of intrinsic defect migration in 3C-SiC, Phys. Rev. B 69 (2004) 245205.
[46] A. García, M.L. Cohen, First-principles ionicity scales. I. Charge asymmetry in the solid state, Phys. Rev. B 47 (8) (1993) 4215.